Analyst

PAPER

View Article Online
View Journal | View Issue

Cite this: *Analyst*, 2024, **149**, 1121

Zwitterionic oligomers of 3-aminobenzoic acid on screen-printed electrodes: structure, properties and forensic application†

Tatiana V. Shishkanova, [a] Eva Pospíšilová, *[a] Miroslava Trchová [b] and Gabriela Broncová [a]

Received 6th October 2023,
Accepted 19th December 2023

DOI: 10.1039/d3an01700a

rsc.li/analyst

The popularity and rapid spread of new psychoactive substances is why there is an urgent need for their fast monitoring in saliva in the field with electrodes modified with a selective receptor. Oligomers of electrochemically oxidized 3-aminobenzoic acid that are deposited on the surface of a graphite screen-printed electrode (o-3ABA/G/SPE) is proposed as a selector for the analyte of forensic interest. The oligomeric structure and existence of the zwitterionic form of o-3ABA on the G/SPE surface was confirmed using scanning electron microscopy, Raman spectroscopy and cyclic voltammetry techniques. The equilibrium adsorption constants between o-3ABA and 2-aminoindane (primary amine: K_{ads}(2-AI) = 5.31 × 10^4) and selected synthetic cathinones (secondary amine: K_{ads}(butylone) = 6.12 × 10^5, tertiary amines: K_{ads}(MDPV) = 3.41 × 10^4 and K_{ads}(naphyrone) = 1.01 × 10^4) were estimated using the electrochemical impedance spectroscopy (EIS) technique. The EIS technique was applied for determining a 1.0 μM concentration of 2-AI (RSD 3.5–4.0%) and butylone (RSD 4.9–6.4%) in the model and oral fluid samples.

Introduction

New psychoactive substances (NPSs) are a complex group of analytes that mimic the effects of known drugs and are often considered 'legal' alternatives. Their growing popularity and rapid spread are reasons for alarm.[1] For example, the stimulating effects of synthetic cathinones (SCs), one of the largest group of NPSs, can be quickly replaced by adverse side effects such as severe anxiety, paranoia, and psychosis.[2] Between 2019 and 2022, 29 new synthetic cathinones were detected for the very first time.[3] Another group of NPSs – aminoindanes – became popular when mephedrone (a class of SCs) was added to the list of controlled substances in the United Kingdom.[4] The effects of aminoindanes have not been sufficiently studied, and therefore pose a great risk to human health. Hence, there is a need for fast and reliable methods for monitoring NPSs, regardless of the sample matrix. Currently, chromatographic methods are often used for a definitive identification of SCs in forensic laboratories.[5] While these methods are sensitive and reliable, they also come with several drawbacks, including long analysis times, the need for expensive equipment, and/or complicated sample preparation. It is important to develop a preliminary identification of SCs using screening tests, in which electrochemical sensors could be an alternative to colorimetric tests.

So far, a number of articles have been published on the detection of NPSs.[6,7] Table 1 presents the progress in the use of electrochemistry for the detection of SCs. Although the use of potentiometry with ion-selective electrodes has been reported,[8–10] most of the electrochemical methods used in these studies were voltammetric methods based on the use of different unmodified and modified electrodes.[5,11–22] The use of unmodified working electrodes often leads to overlapping signals of structural analogues, and therefore limits the selectivity of voltammetric detection. Modification of the electrode surface with a selective receptor, nanoparticles or a polymeric film, is a way to improve the electrochemical signal of individual SCs and to achieve their selective determination. There is indeed an improvement in the limit of detection (LOD) achieved by using modification either with enzymes,[16] aptamers,[15] or nanoparticles[21] (Table 1). Molecular imprinted polymers have gained popularity over the last two decades for the determination of SCs.[13,14,23] Moreover, the selectivity of the modified electrodes enables their applicability in biological samples (blood serum,[14] plasma, urine[13,21] and oral fluids[9]). Additionally, electrochemically synthesized polymers with recognition sites have contributed to the development of electrochemical sensors that have found various appli-

[a]*Department of Analytical Chemistry, University of Chemistry and Technology Prague, Technická 5, 16628 Prague 6, Czech Republic. E-mail: eva.pospisilovavscht.cz*
[b]*Central Laboratory, University of Chemistry and Technology Prague, Technická 5, 16628 Prague 6, Czech Republic*

† Electronic supplementary information (ESI) available. See DOI: https://doi.org/10.1039/d3an01700a

Table 1 An overview of electrochemical sensors used for the detection of synthetic cathinones

Method	Electrode	Analyte	LR, μM	LOD, μM	Real sample	Ref.
Unmodified electrodes						
CV	G/SPE	4-MMC	0–935	55.2	Seized samples	17
CV	G/SPE	4-MEC	0–878	50.9	Seized samples	17
DPV	G/SPE	Eutylone	2–10 2–400	0.33	Seized samples	18
AdSDPV	G/SPE	MDPV	0.2–100	0.5	Seized sample	12
AdSDPV	BDD/SPE	NEP	1–100	0.66	Seized sample	19
SWV	BDDE	Ethylone	13–88	3.7	Seized samples	11
Modified electrodes						
DPV	CNF/SPE	MDPT	0.5–112	0.39	Seized samples	20
DPV	CYP_2D_6/C/SPE	α-PVP	$10–125 \times 10^{-3}$	9.9×10^{-3}	—	16
SWV	MIP/C/SPE	MDPV	—	1.8	Blood serum	14
SWV	Sol–gel-MIP/GCE	4-MMC	$1–10 \times 10^{-3}$	0.8×10^{-3}	Plasma, urine	13
SWV	AgNPS@Sa-CPE	4-MMC	$0.1–4.5 \times 10^{-4}$	3.4×10^{-6}	Urine	21
AdSSWV	C/SPE with surfactant adsorption	Cl-PVP	2.5–30	1.6	Oral fluid[a]	22
AdSDPV	GP/SPE	4-MMC	2.6–112	0.3	Seized samples	5
Pot	ISE	4-MMC	3.3–560	1.0	Oral fluid	9
Pot	ISE	MABP	98–3500	—	Mixture of NPS	10

[a] Cl-PVC was tested in oral fluid, but its detection was affected by oral fluid interferents. **Methods** – AdSDPV: adsorptive stripping different pulse voltammetry. SWV: square-wave voltammetry. CV: cyclic voltammetry. Pot: potentiometry. **Electrodes** – G/SPE: graphite screen-printed electrode. C/SPE: carbon screen-printed electrode. GCE: glassy carbon electrode. BDD/SPE: boron-doped diamond screen-printed electrodes. BDDE: boron-doped diamond electrode. CPE: constant phase element. CNF/SPE: carbon nanofiber screen-printed electrodes. GP/SPE: graphene screen-printed electrodes. ISE: ion-selective electrode. **Modification** – MIP: molecularly imprinted polymer. AgNPS@Sa: silver nanoparticles capped with saffron. CYP_2D_6/C/SPE: carbon screen-printed electrodes modified with CYP_2D_6 enzyme. **Analytes** – 4-MMC: mephedrone. 4-MEC: 4-methylethcathinone. MDPV: 3,4-methylenedioxypyrovalerone. NEP: *N*-ethylpentylone. MDPT: 3′,4′-methylenedioxy-*N*-*tert*-butylcathinone. α-PVP: 4-chloro-alpha-pyrrolidinovalerophenone. MABP: buphedrone.

cations.[24] Xu *et al.* applied a poly(*para*-aminobenzoic acid) (PABA) electrochemically modified glassy carbon electrode coupled with high-performance liquid chromatography to detect dopamine (DA) in a rat brain dialysate.[25] The PABA-modified electrode exhibited excellent catalysis of the electrochemical oxidation of dopamine. Pandey *et al.* utilized electrochemically synthesized poly(indole-6-carboxylic acid) (PICA) for the selective oxidation of DA.[26] With a PICA-modified glassy carbon electrode, the permselectivity for the cations of DA was attributed to the presence of –COOH groups in the polymer backbone. Mahalakshmi and Sridevi prepared a composite of polyaniline (PANI) with Au nanoparticles (AuNPs) on a glassy carbon electrode and so improved its selectivity for DA, applying electrocatalysis simultaneously with the π–π interactions.[27]

This paper shows the use of electrochemically oxidized 3-aminobenzoic acid (3ABA) deposited on graphite screen-printed electrodes for recognizing NPSs, including aminoindane and SCs with primary, secondary, and tertiary amino groups (Fig. 1). A combination of microscopic (scanning electron microscopy) and spectroscopic methods (Raman spectroscopy) was used to determine the morphology and the molecular structure of the 3ABA oxidation products coating the electrode surface. The electrochemical techniques (CV and EIS) enabled estimation of the acid–base character of the oxidation products of 3ABA, their selectivity towards the four NPSs, and then to determine the chosen NPSs, in particular, 2-aminoindane and butylone, in both the model and oral fluid samples.

Experimental

Reagents and materials

Butylone, methylenedioxypyrovalerone (MDPV) and naphyrone, all in forms of hydrochlorides, were acquired by the Forensic Laboratory of Biologically Active Substances (UCT, Prague) from Alfarma s.r.o. 3-Aminobenzoic acid (98%, 3ABA), aniline hydrochloride (97%, Ani) and 2-aminoindane hydrochloride (98%, 2-AI) were obtained from Sigma-Aldrich (USA). Inorganic compounds and acids used for electrochemical measurements were obtained from Lach-Ner or Penta (both Czech Republic, CR). The 0.04 M Britton–Robinson and 0.1 M phosphate buffers were prepared according to the usual protocol from the literature,[28] and the pH was adjusted using solid sodium hydroxide. The solutions were prepared using redistilled water (UCT, Prague).

Apparatus

Cyclic voltammetry (CV) and electrochemical impedance spectroscopy (EIS) measurements were performed using Palmsens 3 (PalmSens BV, Netherlands), controlled by the program PSTrace 5.4. The graphite and gold screen-printed electrodes (3.14 mm^2 working surface; G/SPE and Au/SPE) with Ag/AgCl pseudoreference electrode (BVT Technologies, CR) were used for electrochemical and spectroscopic measurements, respectively.

Raman spectra were collected using a Thermo Scientific DXR Raman microscope equipped with a 780 nm line. The spot size of the lasers was focused with a 50× objective. The scattered light was analyzed with a spectrograph with a holo-

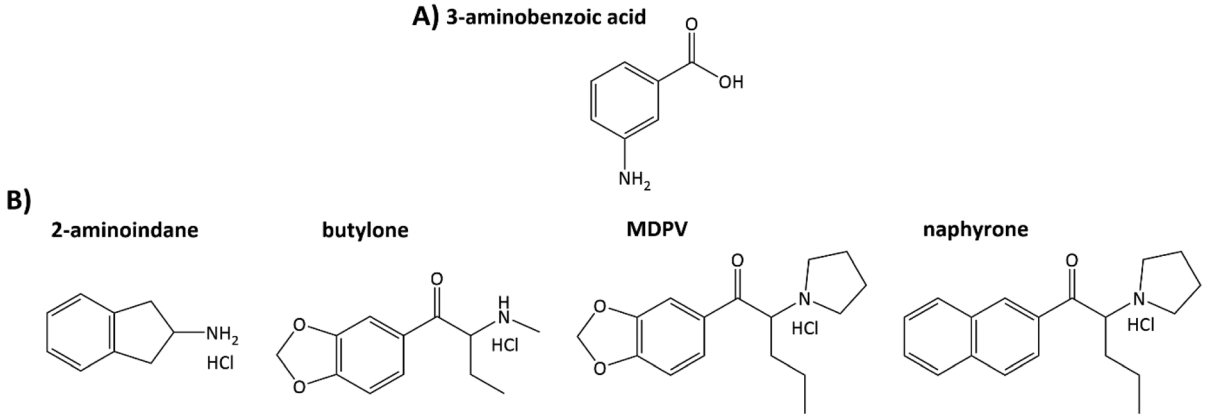

Fig. 1 Structures of 3-aminobenzoic acid (A) and new psychoactive substances chosen for studying (B).

graphic grating of 1200 lines per mm, and a pinhole width of 50 μm. The acquisition time was 10 s with 10 repetitions.

Scanning electron microscopy (SEM) images were recorded with a TESCAN Vega 3XMU InduSem (Tescan Orsay, Czech Republic) scanning electron microscope operating at an accelerating voltage between 15 and 30 kV equipped with a tungsten electron gun at a chamber pressure of 7×10^{-3} Pa. The G/SPEs were coated with a thin chromium film before the SEM measurements.

Electrochemical measurements

Cyclic voltammetry. Prior to use, the G/SPE electrodes were activated by cycling the potential from 0.0 V to +1.5 V (40 cycles) in 0.1 M phosphate buffer with 0.1 M KCl at pH 8. Electrochemical modification of the electrode surface was carried out by CV from the polymerization mixture, which consisted of 50 mM H_2SO_4 and 10 mM 3ABA or Ani. The experimental conditions were as follows: potential range from −0.1 to 1.2 V, a potential step of 0.01 V, scan rate of 50 mV s^{-1}, and 5 scans. According to our laboratory experience, the number of scans (n = 5) enabled us to preserve the undamaged groups that are important for recognizing the analyte of interest and avoid damaging the electrode system during the modification process.[29]

After modification of the G/SPE electrodes, the CV technique was used to evaluate the electrochemical activity and acid–base character (pK_a) of the modified G/SPE electrode in 5 mM $[Fe(CN)_6]^{3-/4-}$ (redox marker) in 0.04 M Britton–Robinson buffer solution of various pH levels over the potential range −0.6 to 0.8 V, and scan rate of 50 mV s^{-1}. The value of the surface pK_a was determined by sigmoid fitting (Boltzmann model) of the peak current to the pH dependence using the program OriginPro 2019b.

Electrochemical impedance spectroscopy. The EIS measurements with both un- and modified G/SPE electrodes were carried out in 0.1 M KCl solution containing 5 mM $[Fe(CN)_6]^{3-/4-}$ (the supporting electrolyte) with or without the analytes of interest. The pH value of the supporting electrolyte varied between pH 5 and 6. The EIS spectra were collected at a potential of 0.0 V in the frequency range from 100 000 to 0.1 Hz, with the amplitude of the applied sine-wave potential being 10 mV. Randles circuits were used for the curve fitting of impedance spectra in the software package PSTrace 5.4. The equivalent circuits consisted of an electrolyte resistance (R_S) in series with a constant phase element (CPE) and charge-transfer resistance (R_{ct}) in parallel. For the G/SPE modified with oxidized 3ABA, the Warburg impedance (W) describing the diffusion of ions to the electrode surface was added in parallel. The R_{ct} values were used to evaluate changes in the electron exchange *via* a redox marker after the modification of the electrode surface in the presence of analytes of interest. The adsorption constant (K_{ads}) values were estimated with a Langmuir adsorption model using the CPE values. To eliminate the electrode-to-electrode discrepancy, the following equation was used: $\Delta CPE = (CPE_n - CPE_0)$, where CPE_0 and CPE_n are the CPE obtained in the supporting electrolyte before and after increasing the concentrations of analytes, respectively. To assess the sensitivity of the modified electrodes, we used the logarithmic dependence, EIS signal = $f(\log(c(\text{NPS})))$, where the EIS signal was obtained from R_{ct} or CPE employing the subsequent equation: EIS signal = $(R_n - R_0)/R_0 \times 1000$ or $(CPE_n - CPE_0)/CPE_0 \times 1000$. The LOD was determined by the following equation: $LOD = 3 \cdot s_y/S$, where s_y is the standard deviation of response and S is the slope of the calibration curve.[30]

Preparation of the model and real samples. Oral fluid (OF) samples (V = 2 ml) were collected from a volunteer (female, 26 years) by letting the oral fluid freely flow into the test tube. Before each sample collection, the volunteer did not eat, smoke or drink anything other than tap water for 30 minutes. Additionally, the oral cavity was rinsed with tap water for one minute. Scheme S1† presents the experimental protocol of the model and oral fluid sample preparation. To prepare the OF samples, 1 ml of the collected OF was spiked with the chosen NPS at a concentration of 1.0×10^{-5} M, and then a redox marker was added and the sample was diluted to 10 ml. With the model samples, 1 ml of distilled water was spiked with the chosen NPS at a concentration of 1.0×10^{-5} M and then processed the same way as that followed for the oral fluid. The con-

centration of the redox marker in this solution was the same as when the concentration dependences were measured, and the NPS concentration in the OF was 1.0×10^{-6} M, which corresponds to a real physiological and forensic situation. This solution (2 ml) was transferred to the measuring cell and a standard addition method was used for NPS determination. The 1 μM sample was spiked multiple times with 0.01 M standard solution of the determined NPSs up to a concentration of 6 μM.

Results and discussion

Electrochemical polymerization of 3-aminobenzoic acid and aniline

Cyclic voltammograms obtained during the electropolymerization of both 3ABA and Ani (used for comparation) on the G/SPE electrode are shown in Fig. 2. Regardless of monomer, the first potential scan shows an irreversible oxidation of the amino group of 3ABA and Ani at +0.85 V and +0.91 V, respectively. The polymerization process is initiated by forming the cation radicals.[31,32] With an increasing number of scans, a decrease in the peak currents was observed for the above-mentioned anodic peaks. This suggests adsorption of the formed oxidation products onto the electrode surface.[33] In the first scan, reduction peaks were observed for both 3ABA (+0.31 V) and Ani (+0.30 V), and the respective oxidation peaks were recorded in the next scan (+0.46 V for 3ABA and +0.35 V for Ani). These peaks correspond to the change in the redox state of the layer deposited on the electrode.[31,32] Compared to Ani, the oxidation/reduction peaks of 3ABA are less defined and only showed a slight increase in current. This phenomenon can be explained by the formation of shorter 3ABA oligomers[34,35] that can be adsorbed onto the electrode surface and thus prevent the redox reaction from occurring.[31]

Electrode characterization

Scanning electron microscopy. The surface morphology of the un- and modified G/SPE electrodes was compared using SEM images (Fig. 3). It was found that the G/SPE surface itself is irregularly porous (Fig. 3A). After the electrochemical oxidation of 3ABA, the G/SPE surface was coated with relatively regular clustered grain/globular motifs of different sizes (Fig. 3B).[36]

This type of coating might correspond to the formation of oligomeric structures rather than polymeric ones.[37] This conclusion can be supported by a proposed series of oligomeric structures for electrochemically oxidized 3ABA (o-3ABA, Scheme S2†).[34] The uniform particle distribution can increase the contact area between the electrolyte and electrode, which may favour electrolyte penetration.[38] The flower-like morphology of PANI/G/SPE (Fig. 3C) is obviously formed due to the acidity of the polymerization media.[37]

Raman spectroscopy. An interpretation of the Raman spectrum of the 3ABA monomer (3ABA, Fig. 4) has recently been provided.[34] The authors assigned the peak with a maximum at 1613 cm^{-1} to the aromatic ring vibration. The absence of the peak of the carbonyl C═O stretching vibration expected at higher wavenumbers signifies the zwitterionic structure of the monomer 3ABA.[39] The peak at 1485 cm^{-1} corresponds to another aromatic ring vibration.[34,40] The strong peak observed at 1386 cm^{-1} belongs to deprotonated COO^- symmetric stretching vibrations.[34,39–41] The peak detected at 1292 cm^{-1} has been assigned to the C–OH stretching vibrations and that at 910 cm^{-1} to the O–H stretching vibrations.[39] The peaks observed at 1229, 1178 and 1010 cm^{-1} are connected with aromatic ring vibrations. The peak at 801 cm^{-1} belongs to the aryl C–H deformation vibrations.[40]

The Raman spectra of electrochemically oxidized 3ABA were measured on the surface of Au/SPE because of a strong scattering on G/SPE. Importantly, the gold surface neither affects the structure nor affects the properties of the deposited materials, which has been recently demonstrated for aniline oligomers.[42,43] The Raman spectrum of oligomers derived from 3ABA (Fig. 4) exhibits a broad baseline, with some of the maxima coming from the monomer. In the Raman spectrum

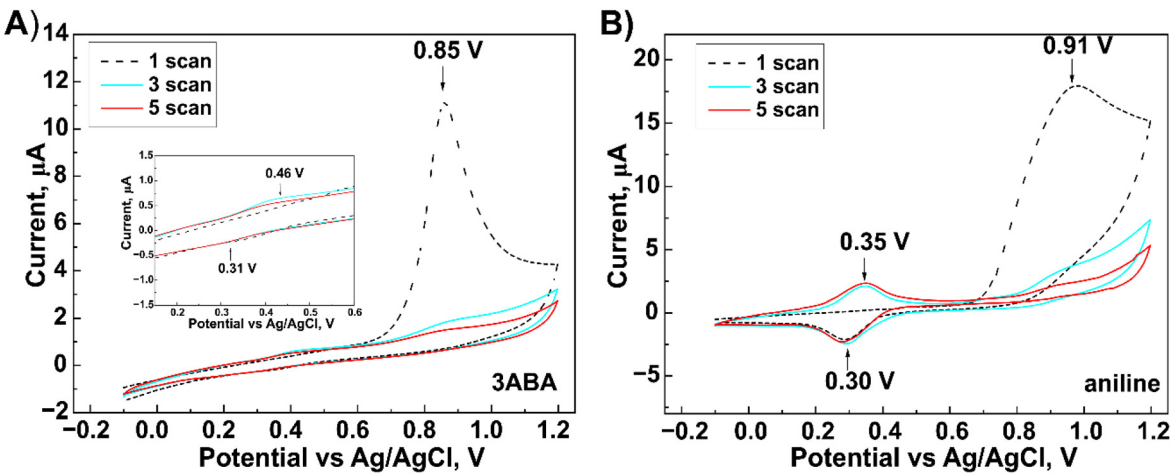

Fig. 2 Cyclic voltammograms obtained during the electrochemical oxidation of 3-aminobenzoic acid (A) and aniline (B) carried out on the surface of graphite screen-printed electrodes.

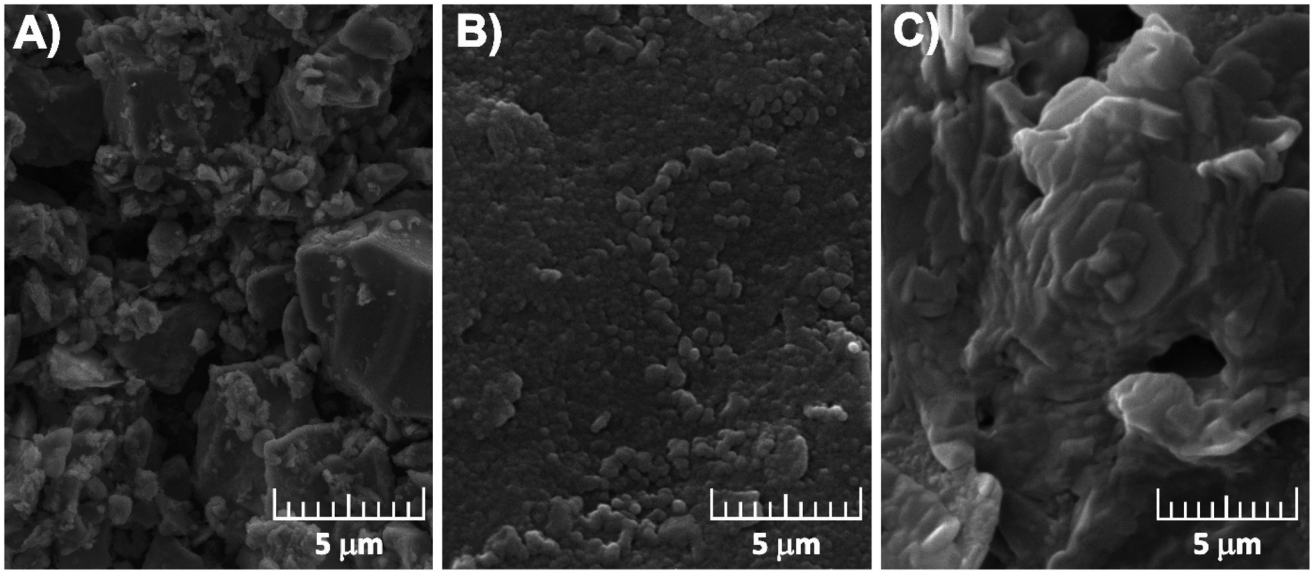

Fig. 3 SEM micrographs of graphite screen-printed electrodes before modification (A) and modified with the oxidation products of 3-aminobenzoic acid (B) and aniline (C).

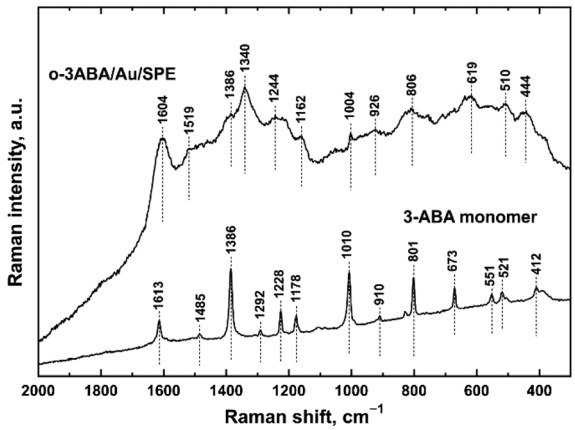

Fig. 4 Dispersive Raman spectra obtained on gold screen-printed electrodes modified with the polymerization product of 3-aminobenzoic acid and the corresponding monomer.

of o-3ABA/Au/SPE, the peak at 1680 cm^{-1} of the acid is also completely absent in the spectrum, which confirms the zwitterionic character of the oxidation product.[41] It is clearly observed that some of the peaks of 3ABA developed into broad bands in the spectrum of o-3ABA/Au/SPE. The band with a maximum at 1604 cm^{-1} can be assigned to aromatic ring vibrations.[34] The maximum at 1519 cm^{-1} has been assigned to the protonated amine symmetric deformation vibrations of NH^+ as stated in ref. 34. A shoulder observed at 1386 cm^{-1} most likely belongs to the COO^- symmetric stretching vibrations.[39,41] A broad band with a maximum at 1340 cm^{-1} assigned previously to the phenol groups represented by the bands of C–O–H deformation vibrations coupled with C–O stretching vibrations, as described in ref. 34, could be connected with the polaron band of newly formed oligomers. Analogous to PANI (Fig. S1†), we suppose that the electrochemical oxidation occurs *via* amino groups and the presence of polarons localized on the molecules of trimers mentioned in ref. 32. The maximum at 1244 cm^{-1} can be attributed to the C–N stretching vibrations. It is clearly seen that the maxima observed at 1162, 1004, 926, and 801 cm^{-1} come from the corresponding peaks present in the spectrum of the monomer. The peak at 510 cm^{-1} corresponds to the deformation vibrations of NH_3^+. Based on the Raman spectroscopic analysis, we confirm the oligomeric structure of the product of electrochemical oxidation of 3ABA *via* amino groups and a zwitterionic form of o-3ABA side groups containing COO^- groups.

Electrochemical impedance spectroscopy. Furthermore, the un- and modified G/SPE were characterized at pH 6 using the EIS method, where the changes in the charge transfer resistances (R_{ct}) and the Warburg impedance were compared. All Nyquist plots show a semicircle that corresponds to R_{ct} in parallel with the CPE (Fig. 5A). The necessity of an application of the CPE (instead of a double layer capacitance, C_{dl}) is explained by the rather rough surface of the un- and modified screen-printed electrodes and defect areas (Fig. 3).[44] The experimental values of R_{ct} changed in the following sequence: G/SPE (34.14 kΩ) < o-3ABA/G/SPE (82.32 kΩ) < PANI/G/SPE (580.95 kΩ) (Fig. 5B). The much larger R_{ct} of the PANI film is a result of the presence of the compact polymeric film with low conductivity that acts as a kinetic barrier to the charge transfer at pH 5–6.[35] The fact that the PANI conductivity is dramatically decreased at pH higher than 4 is well known from the literature.[45] Moreover, there is an obvious and remarkable difference in the conductivity with the G/SPE modified electrodes from the pH dependences measured

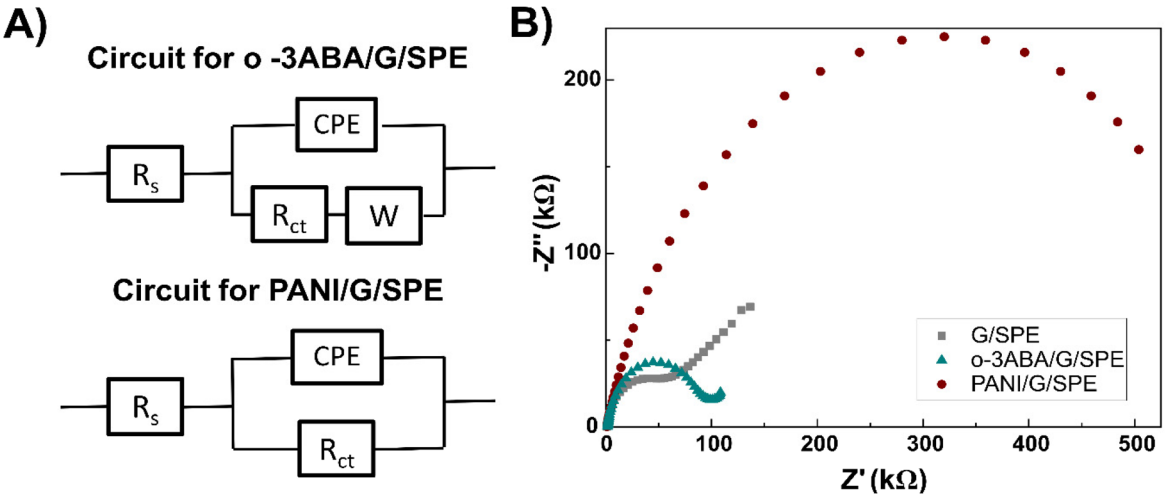

Fig. 5 Equivalent electrical circuits used for the characterization of the modified G/SPE (A) and impedance spectra measured before and after modification of the electrode (B).

using cyclic voltammetry: a higher conductivity for o-3ABA and a small conductivity for PANI at pH 5–6 (Fig. 6). For the o-3ABA/G/SPE, a minor increase in R_{ct} is consistent with the uneven distribution of oligomeric structures on the G/SPE surface. At low frequencies, the Warburg impedance was observed for G/SPE (41.20 kΩ $s^{-1/2}$) and o-3ABA/G/SPE (26.50 kΩ $s^{-1/2}$) that can be associated with the ionic conductivity, random electrode surface heterogeneity, and a partial ionic exchange at the interface between the electrolyte and the electrode surface.[46–48] Additionally, the decrease in the Warburg impedance can be explained by the increased permeability of ions at the polymer–electrolyte interface.[49] The presence of a carboxylate group enhances electron delocalization and facilitates charge transport.[50]

Electrochemical studies

Acid–base character of the modified electrode surface. The next step was studying the pH dependence on the modified G/SPEs using a CV technique (Fig. 6). Knowledge of the acid–base properties of the deposited layers might help to better understand the interactions at the phase boundary of the modified G/SPE and analytes of interest. Different trends were observed in the plots of pH *vs.* current, namely that the current signal increased for o-3ABA and decreased for PANI (Fig. 6 insets). Obviously, both modified surfaces are pH-dependent and possess acidic and basic sites.[32,51] For the PANI film, the pK_a value was 4.13, and indicates the conversion of emeraldine salt to emeraldine base (Fig. 6A). The pK_a value

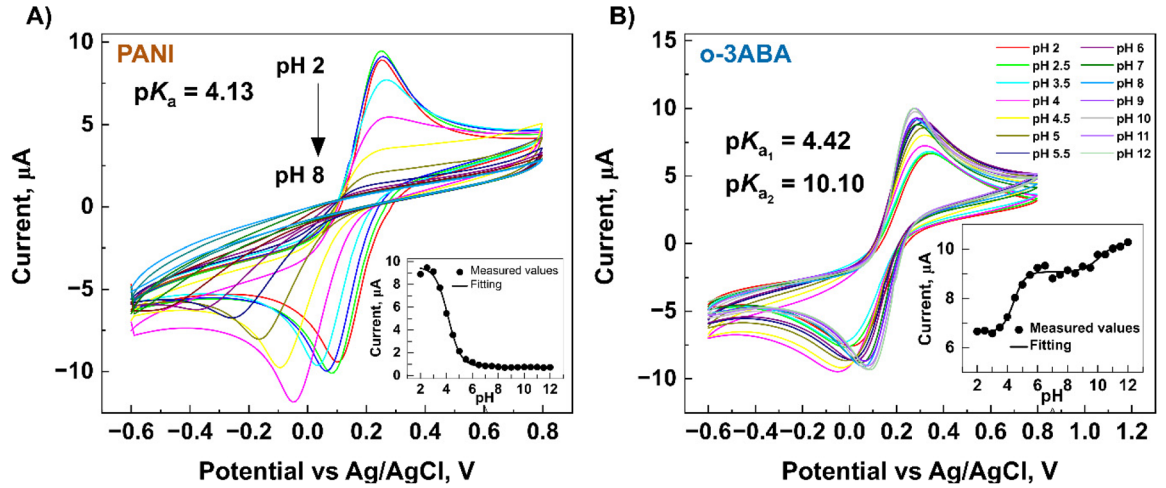

Fig. 6 Cyclic voltammograms obtained for G/SPE modified with PANI (A) and o-3ABA (B) in 0.04 M Britton–Robinson buffer solution of various pH values containing 5 mM $[Fe(CN)_6]^{3-/4-}$. Insets: dependences of peak current on the pH and regression fitting. (Note: Some of the CVs obtained were removed for better visibility of the trend.)

is strongly influenced by the polymerization conditions and was close to the one for polyaniline recorded in ref. 52 (pK_a = 5.42).

3ABA is a unique molecule from the point of view of acid–base ionization properties in a specific pH region in both solution and on the electrode surface. These can be explained by the intramolecular charge transfer (CT) between its amino and carboxyl groups,[50] and because 3ABA possesses a zwitterionic character due to the presence of $–COO^-$ and $–NH_3^+$ groups.[53] For o-3ABA, pK_a = 4.42 and pK_a = 10.10 corresponded to the carboxylic acid and amine groups, respectively (Fig. 6B inset). This confirms that o-3ABA can exist as zwitterionic (moderate pH) and anionic (high pH). The results of CV implicitly showed that o-3ABA is sufficiently conductive to mediate the electron transfer between the redox couple $[Fe(CN)_6]^{3-/4-}$ and G/SPE. It is possible that the oligomeric structures provide an alternative reaction site for the electron transfer processes and are assumed to account for the electrocatalytic reactions.[54] This unique advantage of the presence of zwitterionic groups in o-3ABA might explain the difference between the obtained values of R_{ct} for o-3ABA/G/SPE (82.32 kΩ) and PANI/G/SPE (580.95 kΩ) (Fig. 5B).

Evaluation of the recognition capability of PANI- and o-3ABA-modified electrodes. Langmuir adsorption constants (K_{ads}) obtained from CPE = f(c(analyte)) dependences provided additional insight into the affinity of the modified surface toward the tested analytes (Fig. 7).[55] The K_{ads} values calculated for the PANI layer show its highest affinity for 2-AI (primary amine) and revealed an inability to discriminate between the two tertiary amines. Unlike PANI, the o-3ABA layer was able to distinguish between all tested NPSs, exhibiting the highest affinity for butylone (secondary amine). A significant difference between the ability of the PANI- and o-3ABA-modified electrode to adsorb/recognize 2AI and butylone attracted our attention. As previously proposed, o-3ABA can be considered to be a zwitterionic oligomer, which leads to the coexistence of oppositely charged groups on the modified G/SPE surface. Therefore, the zwitterionic oligomer is able to confer high polarity and hydrophilicity on the surface.[56] The log P values of the chosen NPS exhibited the following sequence of increasing hydrophilicity: naphyrone (1.34) < MDPV (0.05) < butylone (−1.01) < 2-AI (−1.23). This is a possible reason for the higher affinity of o-3ABA for 2-AI/butylone compared to MDPV/naphyrone. Additionally, the interaction between o-3ABA and butylone is supported by specific hydrogen bonding between o-3ABA and the carbonyl and amino moiety of butylone ($–C(O)–CH–NH_2^+–$).

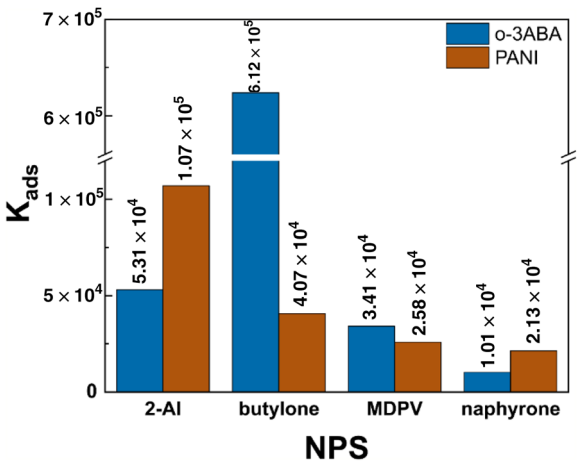

Fig. 7 Comparison of adsorption constant values obtained for the new psychoactive substances with the graphite screen-printed electrode coated with electrochemically oxidized 3-aminobenzoic acid and aniline.

Analytical applicability of o-3ABA-modified electrodes: analytical parameters. A priori, the repeatability of the electrochemical signal for five o-3ABA-modified electrodes was tested and the relative standard deviation (RSD) was in the range from 1.8 to 8.1% (Fig. S2, Table S1†). Next, the EIS response of o-3ABA/G/SPE electrodes obtained with a change in the concentration of 2-AI and butylone was measured and processed at pH 5 to 6 (Table 2, Fig. 8). These pH values are (i) suitable for the o-3ABA-modified surface to be in the form of a zwitterion and (ii) are close to the pH levels of real oral fluids. As shown in Fig. 6, the electrochemical response of the o-3ABA/G/SPE electrode was minimally affected by the pH changes from 5 up to 8. The reproducibility of the height (current intensity) and position (potential) of the peaks for the redox system was 6%.

From the experimental Nyquist plots, it is clear that the semicircles decreased going from low to high concentration. Recently, this phenomenon has been noted in the development of impedimetric biosensors.[55,57,58] The observed decrease in EIS signal has been assigned to less blocking of the flow of electrons through the electrode surface, and has been named as "competitive inhibition assay".[59] A well-defined lower frequency 'tail' is present with butylone, pointing to a better diffusion of butylone toward the electrode surface. Obviously, this diffusion impedance is affected by the structural and transport properties of the heterogenic electrode surface.[48] The calibration equations were calculated from the relative values of circuit elements R_{ct} and CPE (see section "Electrochemical impedance spectroscopy").

For 2-AI, a wide concentration range was obtained for the relationship between the relative value of the CPE and logarithmic value of the concentration dependence. For butylone, the concentration range was shortened. For the detection of the chosen analytes (see section "Analysis of model and oral fluid samples"), we decided to use the values of relative CPE elements from the experimental circuit. In model samples, the limits of detection (LOD) were comparable: 0.92 μM for 2-AI and 0.68 μM for butylone. A deviation of 8.6–13.8% was found at a repeatable calibration of 2-AI and butylone with o-3ABA-modified electrodes (n = 3) in model samples (Table S2†). Such reproducibility is satisfactory considering the low cost of the electrode fabrication route.[60] The interferences of NPSs from the category of synthetic cathinones and substances that can be found in saliva samples (sodium chloride, glucose) were

Table 2 Concentration dependences from EIS measurements for 2-aminoindane and butylone obtained with the experimentally modified o-3ABA graphite screen-printed electrodes

Parameters processed from EIS measurements	NPS	Equation	Linear range (μM)	Correlation coefficient (R^2)
$(R_n - R_0)/R_0 \times 1000$	2-Aminoindane	$-184.3 \log c(\text{2-AI}) - 1336.8$	1–11	0.9948
	Butylone	$-37.2 \log c(\text{But}) - 343.0$	1–711	0.9683
$(\text{CPE}_n - \text{CPE}_0)/\text{CPE}_0 \times 1000$	2-Aminoindane	$-57.2 \log c(\text{2-AI}) - 415.7$	1–922	0.9835
	Butylone	$-37.6 \log c(\text{But}) - 297.8$	1–491	0.9233

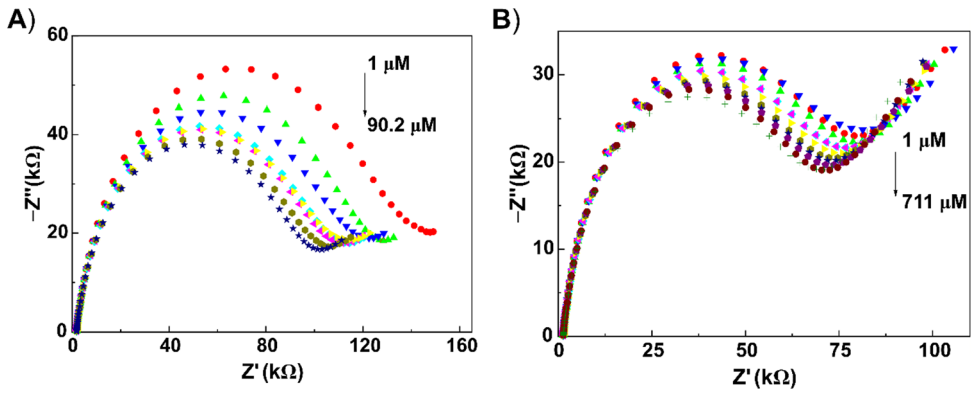

Fig. 8 Electrochemical impedance spectra obtained with electrochemically oxidized 3ABA deposited on graphite electrodes toward 2-AI (A) and butylone (B). Experimental conditions: a supporting electrolyte of 0.1 M KCl containing 5 mM $[Fe(CN)_6]^{3-/4-}$. Concentrations: 1.0 μM (red), 3.0 μM (green), 5.0 μM (blue), 8.0 μM (cyan), 11.0 μM (magenta), 40.8 μM (yellow), 70.5 μM (dark yellow), 90.2 μM (navy), 259 μM (purple), 491 μM (wine) and 711 μM (olive).

then tested (Fig. S3†). The interfering effect increased in the following order:

naphyrone (tertiary amine) < MDPV (tertiary amine) < butylone (secondary amine)

sodium chloride < glucose < 2-aminoindane < butylone.

Importantly, the interfering effect of synthetic cathinones and 2-aminoindane was in agreement with the experimental adsorption constant values (Fig. 7). The fact that the electrode surface is coated with zwitterionic oligomers of 3-ABA explains the minimal interfering effect of charged ions such as sodium and chloride ions. The inter-day stability of the signal at a 1 μM concentration was obtained, and found to be less than one percent (0.7%) for butylone and 2.6% for 2-AI over a span of two weeks (Fig. S4†).

Analytical applicability of the o-3ABA-modified electrodes: an analysis of the model and oral fluid samples. To assess the analytical performance of the experimental o-3ABA electrodes, the determination of 2-AI and butylone was carried out using an EIS technique in spiked model and oral fluid samples (see section "Preparation of the model and real samples").

The most common way of administering synthetic cathinones is through intranasal consumption. Internet user forums report that the dose of NPS that has the pyrrolidine ring and the tertiary amino group can be 5–10 mg.[61] Based on pharmacological studies, the concentration of cathinones in oral fluids is found to vary between 10^{-6} and 10^{-5} M.[62] Oral fluids as samples are an advantageous matrix for NPS determination, since they are easily accessible and can be collected by non-medical personnel. Normal salivary pH is from 6 to 7 and varies in accordance with the salivary flow, from 5.3 (low flow) to 7.8 (peak flow). Moreover, the oral fluids themselves behave as a buffer system.[63] Therefore, the determination of chosen analytes was carried out without addition of a buffer. It was found that both 2-AI and butylone determination was possible with the prepared o-3ABA/G/SPE in both model and oral fluid samples (Table 3, Table S3, Fig. S5†). In oral fluids, the sensitivity and LOD were evaluated: −118 nF decade^{-1}, 1.04 μM for 2-AI; −59 nF decade^{-1}, 0.91 μM for butylone (Table S3, Fig. S5†). The increment in the CPE observed when analysing the oral fluid samples can be explained by the microscopic roughness, chemical inhomogeneities and ion adsorption.[64,65]

Table 3 The results of determination of the 2-aminoindane and butylone (c = 1.0 μM) using impedance spectroscopy with the experimentally modified o-3ABA graphite screen-printed electrodes (n = 5)

Sample	NPSs	Found (μM)	RSD (%)	Recovery (%)
Model sample	2-Aminoindane	0.99 ± 0.04	4.0	99.4
	Butylone	1.02 ± 0.07	6.4	102.0
Oral fluid	2-Aminoindane	1.01 ± 0.03	3.5	100.9
	Butylone	1.03 ± 0.05	4.9	103.1

Table 4 Demonstration of the possibilities of analytical methods for the detection of butylone in samples of forensic interest

Detection method	Sample	Determined concentration (μM)	Ref.
GC-MS	Urine, blood	0.023	68
LC-MS/MS	Postmortem blood	0.003	69
UHPLC-MS/MS	Oral fluid	0.003	70
Square-wave voltammetry with G/SPE	Website samples	10.0	71
EIS with o-3ABA/G/SPE	Oral fluid	1.0	This work

The development of a sensor for application in oral fluids requires the mitigation of biofouling effects. Russo *et al.* have discussed the following strategies for eliminating antifouling: (i) nanoengineered surfaces, (ii) antifouling coatings, (iii) nanoporous membranes and (iv) hydrogels.[66] Zwitterionic compounds can form a strong hydration layer on the surface by interacting with water molecules through hydrogen bonding and electrostatic interaction, which can produce an antifouling effect in an aqueous environment.[67] It can be assumed that zwitterionic oligomers of o-3ABA deposited on the G/SPE surface might be as effective at reducing the fouling and have advantages over the PANI-modified electrode.

Chromatographic methods with mass spectrometry are often used for the laboratory detection of NPSs. While these techniques provide high sensitivity and low detection limits, their main disadvantages are time-consuming sample preparation and analysis. Therefore, it is important to show the possibilities of techniques described in the literature and those proposed in this study (Table 4).

To perform on-site analysis, the sampling step should be coupled with measuring and processing the signal with the corresponding software. Our next steps will be focused on the transfer of our experience and experimental findings in cooperation with a Prague criminology group working in the field of drug analysis.

Conclusions

This manuscript presents a complex characterization of the oligomeric product of 3ABA on the surface of a G/SPE including its morphology, structure and affinity towards the forensic analytes, which included 2-AI and selected synthetic cathinones. The recognizing properties of o-3ABA are dictated by its zwitterionic form that provides high polarity and hydrophilicity to the surface and prefers more hydrophilic butylone ($\log P = -1.01$; K_{ads}(butylone) = 6.12×10^5) and 2-AI ($\log P = -1.23$; K_{ads}(2-AI) = 5.31×10^4). The reason for the higher adsorption constant values for butylone could be additional specific hydrogen bonding occurring between o-3ABA and the butylone molecule. The quantification of 2-AI and butylone at 1.0×10^{-6} M was demonstrated in both the model and oral fluid samples. The modification of surface SPEs is a way to increase the selectivity of voltammetric analysis in the field of forensic praxis.

Author contributions

The manuscript was written through contributions from all authors. All authors have given approval to the final version of the manuscript. Conceptualization: Tatiana V. Shishkanova, Eva Pospíšilová, and Gabriela Broncová; data curation and analysis: Eva Pospíšilová and Miroslava Trchová; writing – original draft: Eva Pospíšilová, Tatiana V. Shishkanova, and Gabriela Broncová; writing – review & editing: Tatiana V. Shishkanova, Eva Pospíšilová, Gabriela Broncová, and Miroslava Trchová.

Conflicts of interest

There are no conflicts to declare.

Acknowledgements

This work was supported by a grant from Specific University Research – Grant No. A2 FCHI 2022 009 and by Institutional Resources (Department of Analytical Chemistry, UCT Prague, CZ; Grant Number: 402850061). The authors are grateful to Dr R. Fajgar for the measurements of the scanning electron microscopy images. The authors are also grateful to Dr M. Kuchař for providing the synthetic cathinones.

References

1 A. Shafi, A. J. Berry, H. Sumnall, D. M. Wood and D. K. Tracy, *Ther. Adv. Psychopharmacol.*, 2020, **10**, 2045125320967197.
2 L. Karila, J. Billieux, A. Benyamina, C. Lançon and O. Cottencin, *Brain Res. Bull.*, 2016, **126**, 61–67.
3 P. Kuropka, M. Zawadzki and P. Szpot, *Forensic Toxicol.*, 2023, **41**, 25–46.
4 C. T. Gallagher, S. Assi, J. L. Stair, S. Fergus, O. Corazza, J. M. Corkery and F. Schifano, *Hum. Psychopharmacol.*, 2012, **27**, 106–112.
5 L. M. A. Melo, L. C. Arantes, I. F. Schaffel, L. M. S. Aranha, N. S. Conceição, C. D. Lima, P. A. Marinho, R. Q. Ferreira and W. T. P. dos Santos, *Analyst*, 2023, **148**, 1552–1561.
6 F. Joosten, M. Parrilla, A. L. N. van Nuijs, K. I. Ozoemena and K. De Wael, *Electrochim. Acta*, 2022, **436**, 141309.

7 B. Zanfrognini, L. Pigani and C. Zanardi, *J. Solid State Electrochem.*, 2020, **24**, 2603–2616.
8 T. V. Shishkanova, E. Pospíšilová and V. Prokopec, *Electroanalysis*, 2022, **34**, 1193–1200.
9 E. Pospíšilová, N. Paškanová, M. Kuchař and T. V. Shishkanova, *Electroanalysis*, 2023, **35**, e202200468.
10 T. V. Shishkanova, L. Vatrsková, D. Spálovská, F. Králík, P. Cuřínová, M. Winkler, J. Budka, B. Jurásek, M. Kuchař and V. Setnička, *Forensic Toxicol.*, 2020, **38**, 70–78.
11 G. L. Scheel, F. M. de Oliveira, L. L. G. de Oliveira, R. A. Medeiros, C. C. Nascentes and C. R. T. Tarley, *Sens. Actuators, B*, 2018, **259**, 1113–1122.
12 C. D. Lima, R. A. S. Couto, L. C. Arantes, P. A. Marinho, D. M. Pimentel, M. B. Quinaz, R. A. B. da Silva, E. M. Richter, S. L. Barbosa and W. T. P. dos Santos, *Electrochim. Acta*, 2020, **354**, 136728.
13 I. Razavipanah, E. Alipour, B. Deiminiat and G. H. Rounaghi, *Biosens. Bioelectron.*, 2018, **119**, 163–169.
14 R. A. S. Couto, C. Coelho, B. Mounssef Jr., S. F. A. Morais, C. D. Lima, W. T. P. dos Santos, F. Carvalho, C. M. P. Rodrigues, A. A. C. Braga, L. M. Gonçalves and M. B. Quinaz, *Nanomaterials*, 2021, **11**(2), 353.
15 Y. Liu, H. Yu, O. Alkhamis, J. Moliver and Y. Xiao, *Anal. Chem.*, 2020, **92**, 5041–5047.
16 A. F. Lugo Vargas, W. G. Quevedo Buitrago, D. C. Chaves Silva and J. F. Martínes Suárez, *ChemistrySelect*, 2022, **7**, e202202748.
17 J. P. Smith, J. P. Metters, O. I. G. Khreit, O. B. Sutcliffe and C. E. Banks, *Anal. Chem.*, 2014, **86**, 9985–9992.
18 M. O. B. Arrieiro, L. C. Arantes, D. A. R. Moreira, D. M. Pimentel, C. D. Lima, L. M. F. Costa, R. M. Verly and W. T. P. dos Santos, *Electrochim. Acta*, 2022, **412**, 140106.
19 L. M. A. Melo, L. V. de Faria, L. C. Arantes, M. Vojs, M. Marton, R. F. Brocenschi, E. M. Richter, R. A. A. Munoz and W. T. P. dos Santos, *Electrochim. Acta*, 2023, **465**, 142996.
20 C. D. Lima, L. M. A. Melo, L. C. Arantes, N. d. S. Conceição, I. de França Schaffel, L. L. Machado, R. de Queiroz Ferreira and W. T. P. dos Santos, *Talanta*, 2024, **269**, 125375.
21 G. C. Papaioannou, S. Karastogianni and S. Girousi, *Sensors*, 2022, **22**, 1625.
22 M. Parrilla, F. Joosten and K. De Wael, *Sens. Actuators, B*, 2021, **348**, 130659.
23 H. Chen, F. Wu, Y. Xu, Y. Liu, L. Song, X. Chen, Q. He, W. Liu, Q. Han, Z. Zhang, Y. Zou and W. Liu, *RSC Adv.*, 2021, **11**, 29752–29761.
24 M. Ates, *Mater. Sci. Eng., C*, 2013, **33**, 1853–1859.
25 F. Xu, M. Gao, L. Wang, G. Shi, W. Zhang, L. Jin and J. Jin, *Talanta*, 2001, **55**, 329–336.
26 P. C. Pandey, D. S. Chauhan and V. Singh, *Electrochim. Acta*, 2009, **54**, 2266–2270.
27 S. Mahalakshmi and V. Sridevi, *Electrocatalysis*, 2021, **12**, 415–435.
28 J. Fogl and K. Volka, *Analytické tabulky*, VŠCHT, Praha, 2 edn, 2002.
29 T. V. Shishkanova and A. Sinica, *J. Electroanal. Chem.*, 2022, **921**, 116674.
30 Determination of limit of detection, **https://arts-sciences.und.edu/academics/chemistry/kubatova-research-group/_files/docs/determination_of_lods_new.pdf**, (accessed 05.11.2023).
31 Y. T. Liu, J. Deng, X. L. Xiao, L. Ding, Y. L. Yuan, H. Li, X. T. Li, X. N. Yan and L. L. Wang, *Electrochim. Acta*, 2011, **56**, 4595–4602.
32 G. Ćirić-Marjanović, *Synth. Met.*, 2013, **177**, 1–47.
33 P. C. M. Santos, T. M. Lima, P. I. Soares, R. M. Coelho, H. R. Martins, D. B. da Cruz, A. C. Pereira, D. L. Franco and L. F. Ferreira, *Mater. Chem. Phys.*, 2022, **288**, 126364.
34 T. V. Shishkanova, G. Broncová, Z. Němečková, V. Vrkoslav, V. Král and P. Matějka, *J. Electroanal. Chem.*, 2019, **832**, 321–328.
35 C. Thiemann and C. M. A. Brett, *Synth. Met.*, 2001, **123**, 1–9.
36 E. N. Zare, M. M. Lakouraj and E. Moosavi, *Compos. Interfaces*, 2016, **23**, 571–583.
37 Y. Zhao, J. Stejskal and J. Wang, *Nanoscale*, 2013, **5**, 2620–2626.
38 J. Yan, W. Yuan, Z.-Y. Tang, H. Xie, W.-F. Mao and L. Ma, *J. Power Sources*, 2012, **209**, 251–256.
39 M. Samsonowicz, T. Hrynaszkiewicz, R. Świsłocka, E. Regulska and W. Lewandowski, *J. Mol. Struct.*, 2005, **744–747**, 345–352.
40 R. Świsłocka, E. Regulska, M. Samsonowicz, T. Hrynaszkiewicz and W. Lewandowski, *Spectrochim. Acta, Part A*, 2005, **61**, 2966–2973.
41 H. Park, S. B. Lee, K. Kim and M. S. Kim, *J. Phys. Chem.*, 1990, **94**, 7576–7580.
42 M. Trchová, Z. Morávková, J. Dybal and J. Stejskal, *ACS Appl. Mater. Interfaces*, 2014, **6**, 942–950.
43 M. Trchová, Z. Morávková, M. Bláha and J. Stejskal, *Electrochim. Acta*, 2014, **122**, 28–38.
44 T. Balkenhohl and F. Lisdat, *Anal. Chim. Acta*, 2007, **597**, 50–57.
45 A. A. Karyakin, A. K. Strakhova and A. K. Yatsimirsky, *J. Electroanal. Chem.*, 1994, **371**, 259–265.
46 M. Vrňata, D. Kopecký, F. Vysloužil, V. Myslík, P. Fitl, O. Ekrt, J. Hofmann and L. Kučera, *Sens. Actuators, B*, 2009, **137**, 88–93.
47 S. Dhillon and R. Kant, *J. Chem. Sci.*, 2017, **129**, 1277–1292.
48 J. Huang, *Electrochim. Acta*, 2018, **281**, 170–188.
49 A. Yavarinasab, M. Abedini, H. Tahmooressi, S. Janfaza, N. Tasnim and M. Hoorfar, *Polymers*, 2022, **14**, 31.
50 T. Stalin and N. Rajendiran, *Chem. Phys.*, 2006, **322**, 311–322.
51 C. Anex, E. Touzé, L. Curet, F. Gohier and C. Cougnon, *ChemElectroChem*, 2019, **6**, 4963–4969.
52 W. Gao and J. Song, *Electroanalysis*, 2009, **21**, 973–978.
53 S. H. Hilal, S. W. Karickhoff and L. A. Carreira, *Talanta*, 1999, **50**, 827–840.
54 A. M. Asiri, W. A. Adeosun, H. M. Marwani and M. M. Rahman, *New J. Chem.*, 2020, **44**, 2022–2032.

55 T. V. Shishkanova, F. Králík and A. Synytsya, *Sensors*, 2023, **23**, 3727.
56 K. Qu, Z. Yuan, Y. Wang, Z. Song, X. Gong, Y. Zhao, Q. Mu, Q. Zhan, W. Xu and L. Wang, *Chem. Phys. Mater.*, 2022, **1**, 294–309.
57 J. Zhang, Y. Wu, B. Zhang, M. Li, S. Jia, S. Jiang, H. Zhou, Y. Zhang, C. Zhang and A. P. F. Turner, *Anal. Lett.*, 2012, **45**, 986–992.
58 J. V. Rushworth, A. Ahmed, H. H. Griffiths, N. M. Pollock, N. M. Hooper and P. A. Millner, *Biosens. Bioelectron.*, 2014, **56**, 83–90.
59 E. P. Randviir and C. E. Banks, *Anal. Methods*, 2013, **5**, 1098–1115.
60 J. R. Sempionatto, T. Nakagawa, A. Pavinatto, S. T. Mensah, S. Imani, P. Mercier and J. Wang, *Lab Chip*, 2017, **17**, 1834–1842.
61 EMCDDA, Synthetic cathinones drug profile, **https://www.emcdda.europa.eu/publications/drug-profiles/synthetic-cathinones_en**, (accessed 19.11.2023).
62 E. Papaseit, E. Olesti, C. Pérez-Mañá, M. Torrens, F. Fonseca, M. Grifell, M. Ventura, R. de la Torre and M. Farré, *Pharmaceuticals*, 2021, **14**, 100.
63 P. D. V. De Almeida, A. M. T. Grégio, M. Â. N. Machado, A. A. S. De Lima and L. R. Azevedo, *J. Contemp. Dent. Pract.*, 2008, **9**, 072–080.
64 J. S. Daniels and N. Pourmand, *Electroanalysis*, 2007, **19**, 1239–1257.
65 J.-B. Jorcin, M. E. Orazem, N. Pébère and B. Tribollet, *Electrochim. Acta*, 2006, **51**, 1473–1479.
66 M. J. Russo, M. Han, P. E. Desroches, C. S. Manasa, J. Dennaoui, A. F. Quigley, R. M. I. Kapsa, S. E. Moulton, R. M. Guijt, G. W. Greene and S. M. Silva, *ACS Sens.*, 2021, **6**, 1482–1507.
67 J. Niu, H. Wang, J. Chen, X. Chen, X. Han and H. Liu, *Colloids Surf., A*, 2021, **626**, 127016.
68 L. A. Nisbet, F. M. Wylie, B. K. Logan and K. S. Scott, *J. Anal. Toxicol.*, 2019, **43**, 346–352.
69 T. Lau, M. Concheiro and G. Cooper, *J. Anal. Toxicol.*, 2020, **44**, 679–687.
70 M. Williams, J. Martin and P. Galettis, *J. Anal. Toxicol.*, 2017, **41**, 659–669.
71 J. Schram, M. Parrilla, N. Sleegers, F. Van Durme, J. van den Berg, A. L. N. van Nuijs and K. De Wael, *Drug Test. Anal.*, 2021, **13**, 1282–1294.